Available online at www.sciencedirect.com
SCIENCE DIRECT
Journal of Catalysis 236 (2005) 262–269
JOURNAL OF CATALYSIS
www.elsevier.com/locate/jcat

Reaction mechanism of preferential oxidation of carbon monoxide on Pt, Fe, and Pt–Fe/mordenite catalysts

Masashi Kotobuki [a], Akiko Watanabe [a], Hiroyuki Uchida [a], Hisao Yamashita [b], Masahiro Watanabe [b,*]

[a] *Interdisciplinary Graduate School of Medicine and Engineering, University of Yamanashi, Takeda 4, Kofu 400-8510, Japan*
[b] *Clean Energy Research Center, University of Yamanashi, Takeda 4, Kofu 400-8510, Japan*

Received 7 June 2005; revised 8 August 2005; accepted 21 September 2005

Available online 7 November 2005

Abstract

We have investigated the preferential oxidation (PROX) of carbon monoxide at Pt/mordenite (Pt/M), Fe/mordenite (Fe/M), and Pt–Fe/mordenite (Pt–Fe/M) for a purification of reformates to supply polymer electrolyte fuel cells (PEFCs). Pt–Fe/M exhibited remarkable PROX activity up to an extremely high space velocity (i.e., ca. 100% selectivity, SV $= \sim 10^5$ h^{-1}) even at 50 °C, although Pt/M and Fe/M had negligibly small PROX activity. CO, H_2, and O_2 chemisorption measurements demonstrated that Pt sites act as adsorption sites for CO and/or H_2 and Fe (dominantly FeO) sites only for O_2, so that the addition of Fe to Pt/M can preserve O_2 adsorption sites for the PROX reaction even in CO/excess H_2 gas flow. The poor reactivity of Pt/M and Fe/M can be ascribed to the lack of CO and/or O_2 adsorption as the essential requisite for the Langmuir–Hinshelwood mechanism. We propose the so-called "bifunctional mechanism" for the distinctive performance at Pt–Fe/M, where the Pt site acts as a CO adsorption site and the Fe site acts as an O_2 dissociative-adsorption site and enhances the surface reaction between the reactants on the neighboring sites.

Keywords: Preferential oxidation; Selective oxidation; Carbon monoxide; Zeolite catalyst; Hydrogen purification; Fuel cell

1. Introduction

Fuel cells are clean, high-efficiency power generation systems. Polymer electrolyte fuel cells (PEFCs) are being extensively developed as power sources for electric vehicle and residential cogeneration, portable electric devices, and other uses. Hydrogen is the most desirable fuel for PEFCs because of its reactivity. One of the most realistic production hydrogen methods is the reforming of hydrocarbon fuels, such as natural gas, gasoline, kerosene, or methanol, followed by a CO shift reaction to form H_2-rich fuel gases. However, such reformates still contain 1% level CO [1]. Because the anode Pt catalyst in PEFCs is very sensitive to poisoning by CO, particularly at low operating temperatures, the concentration of CO must be reduced to, say, $<$10 ppm [2].

In terms of the choice for purification, preferential oxidation (PROX) of CO by O_2 supplied to the fuel stream has been proposed for removing CO from the reformates. PROX is advantageous over the existing other technologies, such as membrane separation or pressure swing methods, because it can operate at relatively low temperatures and atmospheric pressure, resulting in a compact reforming system that can quickly response to load changes and frequent starting and stopping of the operation [3]. In this process, suppression of H_2 oxidation or methane formation accompanying the H_2 loss is essential to achieve high PEFC system efficiency. Therefore, high-performance PROX catalysts are required that can be operated with the minimized molar ratio of O_2 to CO ($\lambda = 2 \times O_2/CO$) and high selectivity to CO oxidation. Such an operation is also important from the standpoint of managing the heat in the PROX reactor, by eliminating H_2 oxidation with excess O_2.

Until now, many researchers have studied the PROX catalysts, such as noble metal catalysts supported on some ox-

* Corresponding author. Fax: +81 55 254 0371.
E-mail address: m-watanabe@yamanashi.ac.jp (M. Watanabe).

0021-9517/$ – see front matter
doi:10.1016/j.jcat.2005.09.026

ides [4–10] or carbon [11]. We first proposed zeolite catalysts loaded with Pt or the alloys for the PROX reaction, intending to use zeolite pores as the special reaction spaces [12]. Because they have larger molecular weights and also higher chemisorbing properties than H_2, CO and O_2 are expected to remain longer and thus have a greater chance of being adsorbed on catalysts in the pores than do conventional alumina-supported catalysts. Accordingly, zeolite-supported catalysts are expected to selectively promote CO oxidation. We prepared Pt or Pt alloy catalysts in zeolite cages in a highly dispersed state by applying the ion-exchange method for the metallic sources, followed by reduction with H_2 gas. We found that 4 wt% Pt–2 wt% Fe/mordenite (mordenite-supported) exhibited better activity and selectivity than Pt–Fe/mordenite with other metallic compositions pretreated at 500 °C, and much better activity and selectivity than any other single or Pt base bimetallic catalysts supported on various zeolites pretreated at the same 500 °C [12–15]. Moreover, we found that the PROX performance of Pt/ZSM-5 was improved by lowering the pretreatment temperature from 500 to 300 °C [16]. Thus we applied this low preheating temperature to Pt–Fe/mordenite catalysts with various compositions and found that 4 wt% Pt–0.5 wt% Fe/mordenite catalyst demonstrated the best PROX performance among them.

In the present work we first demonstrate the superior PROX performance on this 4 wt% Pt–0.5 wt% Fe/mordenite catalyst. We then discuss the catalysis mechanism, based on studies applying the adsorption/desorption measurements on the catalyst in comparison with those of Pt/mordenite and Fe/mordenite.

2. Experimental

2.1. Catalyst preparation

Pt^{2+} and Fe^{3+} were supported on a Na-type mordenite (a reference sample supplied by the Catalysis Society of Japan, denoted as M) by a conventional ion-exchange method [12–14]. First, the M powders were added into aqueous solution of $[Pt(NH_3)_4]Cl_2$ (Tanaka Kikinzoku Kogyo K.K.) and stirred at room temperature for Pt^{2+} exchanging adsorption. After 15 h, the suspension was filtered. The filtrated M was then added into $Fe(NO_3)_3$ aqueous solution, stirred for Fe^{3+} exchange for 48 h at 50 °C and filtered. The obtained samples were washed well with deionized water, followed by drying at 60 °C for 24 h. The resulting cakes were crushed to powders and sieved. The 100- to 200-mesh powders were stored in a desiccator. The amounts of supported metals were determined with ICP (Seiko SPQ9000) by measuring Pt and Fe concentrations in the filtrates. The resulting loading amounts of Pt and Fe were 4 wt% and 0.5 wt%, respectively. For the comparison, mordenite catalysts loading single Pt or Fe in 4 wt% and 0.5 wt%, respectively, were also prepared in a similar manner as the Pt–Fe supporting catalyst. These catalysts were denoted by Pt/M, Fe/M, and Pt–Fe/M, respectively.

2.2. Activity test

PROX activity tests were carried out in a conventional flow reactor [12–14]. The 50-mg supported catalysts were mounted in a Pyrex tube reactor (6 mm i.d.). Reaction gas containing 1% CO, 0.5% O_2, and H_2 balance was prepared by mixing H_2 containing 1% CO and pure O_2 using two mass flow controllers. In a practical PROX reaction, H_2O and CO_2 should be included. In the previous work [15], however, we studied the effect of their presences on the PROX properties and found no noticeable degradation of the properties. At the PROX reaction process in zeolite cages, the exothermic reaction may suppress condensation of H_2O in the cages. Therefore, we use the reactant gas composition without H_2O and CO_2 in the present work, because the main purpose of this work is the discussion of the PROX mechanism. Reaction temperature was measured with a thermocouple attached to the outer wall of the reactor tube. Space hourly velocity (SV), the ratio of total gas volumetric flow rate to the catalyst volume mounted in the reactor tube, was used as an index of catalyst performance. An on-line gas chromatograph with a thermal conductivity detector (TCD) (Hitachi GC 263-30) was used to measure inlet and outlet gas composition. A 13X molecular sieve column was used to separate oxygen, methane, and carbon monoxide, and an active carbon column was used to analyze carbon dioxide.

The CO conversion, O_2 conversion, and selectivity were defined as follows:

$$\text{CO conversion (\%)} = [CO_2]/[CO]_0 \times 100,$$

$$O_2 \text{ conversion (\%)} = ([O_2]_0 - [O_2])/[O_2]_0 \times 100,$$

$$\text{Selectivity (\%)} = 0.5 \times [CO_2]/([O_2]_0 - [O_2]) \times 100,$$

where $[CO_2]$ is the concentration of CO_2 in product gas, $[CO]_0$ is the inlet carbon monoxide concentration, and $[O_2]_0$ and $[O_2]$ are the oxygen concentrations at the inlet and outlet, respectively. All of the data were recorded at the steady state. Before the activity test, each catalyst was treated in O_2 flow at 300 °C for 1 h and switched to N_2 flow. After 30 min in N_2 flow, the catalyst was treated in H_2 flow for 1 h at 300 °C. This treatment is called "H_2 pretreatment" in this paper.

2.3. Characterization

The Pt–Fe/M sample after the activity test was observed by transmission electron microscopy (TEM) (Hitachi HD-2000) operating at 200 kV. The Pt–Fe/M powders were embedded in a resin. After the resin hardened, it was sliced by a microtome for preparation of test pieces. Then TEM observation was performed.

The BET surface area of the catalysts was determined with the adsorption capacity of nitrogen using N_2 physisorption equipment (Bel Japan BEL-mini). Before measurement, each catalyst sample was heat treated for the conditioning in a conventional manner. Then nitrogen adsorption on the sample was measured at liquid nitrogen temperature. For comparison with the catalyst samples, the BET surface area of mordenite itself, used as the catalyst support, was also measured.

Affinities of Pt/M, Fe/M, and Pt–Fe/M catalysts to CO, H_2, and O_2 adsorption were examined using commercial chemisorption equipment (Bel Japan BEL-METAL4) as follows. Each ion-exchanged catalyst was first placed in a Pyrex tube, then H_2 pretreated under the conditions described in Section 2.2. After pretreatment, the sample was cooled to each measurement temperature in He flow. Then a CO, O_2, or H_2 pulse was introduced until the saturated coverage was achieved. The effluent gas through the catalyst bed was detected by a TCD. During the test, He gas for CO and O_2 adsorption and Ar gas for H_2 adsorption were used as carrier gases. The amount of each chemisorbed gas was calculated from the integration of the reduced peak areas of detected pulses, corresponding to Fig. 4.

Competitive adsorption of CO and H_2 from the mixed gases was also determined by exposing Pt/M and Pt–Fe/M catalysts at 50 °C in a gas flow containing 0.5% CO, 5% H_2, and He balance for 1 h. Temperature-programmed desorption (TPD) profiles of CO and H_2 were collected with a commercial catalyst analyzer (Bel Japan BEL-CAT) equipped with a mass spectrometer by heating up to 400 °C at a 10 °C/min ramp rate, corresponding to Fig. 5.

CO adsorption and the oxidative desorption at Pt/M and Pt–Fe/M catalysts were examined at 50 °C, corresponding to Figs. 6 and 7. The samples for the measurement were H_2 pretreated, then cooled to 50 °C in He flow. Then CO (5% CO and He balance) or CO + H_2 (0.5% CO, 5% H_2, and He balance) was pulse-injected in He carrier gas flow until the saturated coverage with CO and/or H_2 was achieved. After the saturation, O_2 was pulse-injected in the same carrier gas flow to evaluate the reactivity between the preadsorbed CO and/or H_2 and the postinjected O_2 at the Pt/M and Pt–Fe/M catalysts. The amounts of CO, H_2, O_2, H_2O, and CO_2 exhausted were monitored with the same BEL-CAT device described above.

3. Results and discussion

3.1. PROX properties of Pt/M, Fe/M, and Pt–Fe/M catalysts

3.1.1. Temperature dependence

Fig. 1 shows PROX properties of Pt/M, Fe/M, and Pt–Fe/M catalysts at SV = 50,000 h^{-1} and $\lambda = 1.0$ (stoichiometric amount of O_2) as a function of reaction temperature. At all of the catalysts, no CH_4 was formed via useless consumption of H_2 reacting with CO or CO_2 over the whole temperature region, which is distinctive from many other catalysts supported on nonzeolite supports. At Fe/M, the PROX reaction hardly occurred in our test conditions. Consistent with our previous observations under different reaction conditions [13,14], Pt/M showed poor PROX performance; that is, the CO conversion commences above 150 °C, although O_2 conversion starts at around 100 °C. Both conversions increase with temperature elevation. The selectivity shows a maximum at ca. 200 °C, but it does not exceed 60%. Wootsch et al. reported similar behavior of CO and O_2 conversion on Pt catalyst supported on γ-Al_2O_3 powder [17]. In contrast, Pt–Fe/M catalyst shows extremely high CO conversion and selectivity distinctive from

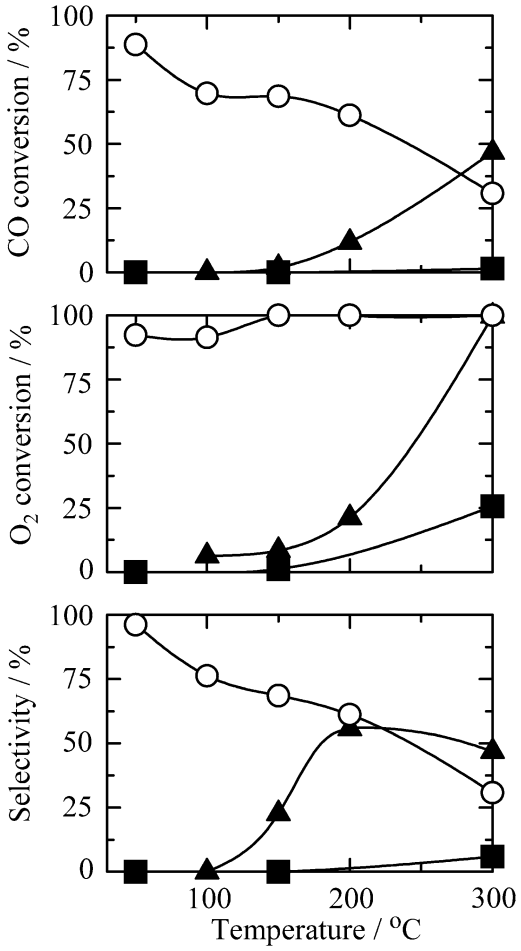

Fig. 1. PROX activity of different catalysts as a function of temperature. Reactant gas: 1% CO, 0.5% O_2, and H_2 balance. Space velocity: 50,000 h^{-1} (▲) 4 wt% Pt/M, (■) 0.5 wt% Fe/M, (○) 4 wt% Pt–0.5 wt% Fe/M.

those of Pt/M and Fe/M, particularly at low temperatures, but similar to our previous results for Pt–Fe/M samples with higher Fe content (Pt/Fe < 3/1) [15]. The CO conversion and selectivity increase with decreasing operating temperature, although O_2 conversion decreases slightly below 150 °C because of decreased direct H_2 oxidation. It must be emphasized that CO conversion and selectivity exceed 90 and 95%, respectively, even with the stoichiometric O_2 supply ($\lambda = 1.0$) and an operating temperature as low as 50 °C, which is very desirable for cold starting of fuel cells.

3.1.2. Space velocity dependence

The ability to achieve good PROX performance at a high SV condition as well as the minimum λ (=1.0) at even low temperatures is critical for a compact and quickly responsible PROX reactor. Fig. 2 shows the effect of SV values on the PROX performances of Pt–Fe/M catalyst at 50 °C and $\lambda = 1.0$. CO and O_2 conversion and selectivity at SV = 12,500 h^{-1} are almost 100%. CO selectivity is suppressed slightly by increasing SV value but nonetheless maintains a surprisingly high value of ca. 95% at 100,000 h^{-1} under our operating conditions. The mechanism responsible for such remarkable PROX behavior is discussed in detail below.

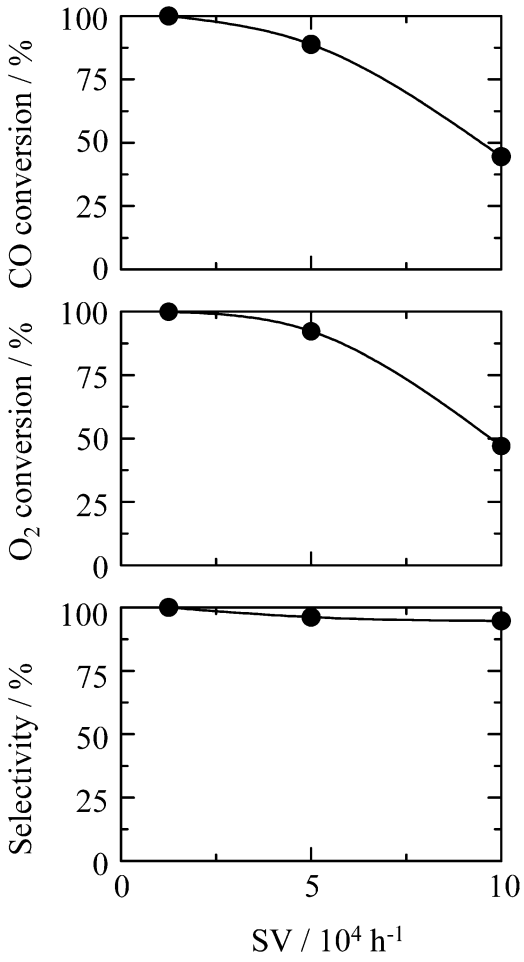

Fig. 2. PROX activity on 4 wt% Pt–0.5 wt% Fe/M as a function of space velocity. Reactant gas: 1% CO, 0.5% O_2, and H_2 balance, reaction temperature: 50 °C.

Table 1
BET surface area of various catalysts

	Catalyst			
	Pt/M	Fe/M	Pt–Fe/M	M
Surface area (m^2/g_{cat})	407	404	392	408
Surface area (m^2/g_M)[a]	424	406	411	408

[a] Assuming that Fe was in FeO phase.

3.2. Role of each catalyst site for reactant adsorption and reaction

As mentioned here and in our previous papers [12–15], the Pt–Fe/M catalyst shows superior performance for the PROX reaction than the other catalysts and/or supports. We have proposed a possible mechanism to explain this superiority; however, neither the behavior itself nor the mechanism has yet been clarified. To investigate this mechanism, we further characterize the catalyst in the present work.

3.2.1. Catalyst surface area

Table 1 shows BET surface areas of H_2-pretreated Pt/M, Fe/M, Pt–Fe/M, and the support M. Our previous XANES analysis on H_2-pretreated Pt–Fe/M catalysts with different Fe-contents indicated that in the mordenite cages, Pt exists in the metallic state, but Fe resembles FeO predominantly [18]. Therefore, surface areas normalized with 1 g mordenite are calculated and shown in the same table, assuming that Fe is all in the FeO phase, although this is hardly reflected in the resulting surface areas. An increase in the normalized BET surface areas by loading catalysts on M, which must be ascribed to the surface areas of metal catalysts, is almost hidden within experimental errors due to the extremely high surface area of the M support itself. So the difference in surface areas among metallic catalysts is beyond the scope of this discussion of PROX behavior. Nevertheless, it is reasonable to consider that the difference might be small, because major parts of the catalyst surfaces are located inside the support cages. Fig. 3 shows a typical TEM photograph of a sliced sample of 4 w% Pt–0.5 w% Fe/M after the PROX reaction. Based on our previous work [15,16], we have concluded that the large particles observed on a periphery of each sliced sample are the catalysts supported on the viewing mordenite surface and that the small particles inside are the catalysts supported in the mordenite cages. This photograph looks very similar to both TEM photos of other views of the present sample and TEM photos of the 4 wt% Pt–2 wt% Fe/M pretreated at 500 °C [15] or 6 wt% Pt/ZSM-5 pretreated at 300 °C [16]. Thereby, the ratio of the total surface areas of small metallic particles to the total surface areas of the metallic particles including the large particles are evaluated by counting particle numbers and their particle sizes, that is, several hundreds of the small and large particles on several photographs. As a result, it was found that metallic catalyst areas of ca. 85%, 80%, and 83% are located inside each zeolite cage at 4 w% Pt–0.5 w% Fe/M, 4 wt% Pt–2 wt% Fe/M, and 6 wt% Pt/ZSM-5, respectively. Previous work [16] clearly demonstrated that such small particles insides the zeolite cages play the dominant role in the selectivity to CO oxidation and the high reaction rate in the PROX reaction. These properties must result from the high specific surface areas of small catalyst particles and the special reaction environment in zeolite cages, although the wt% of the small particles to the large particles is relatively small.

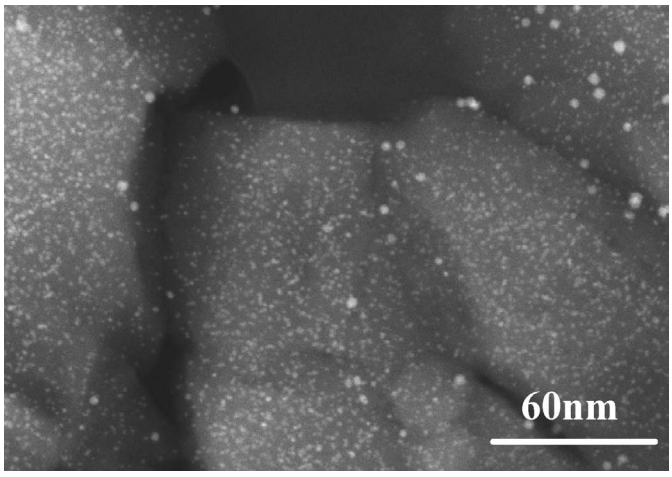

Fig. 3. TEM image on Pt–Fe/M catalyst after PROX activity test.

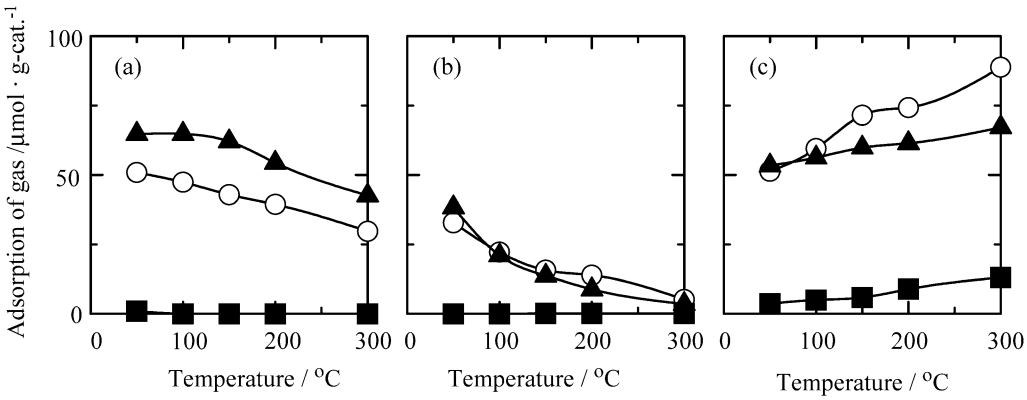

Fig. 4. Saturating amounts of (a) CO, (b) H_2 and (c) O_2 adsorbed on (▲) Pt/M, (■) Fe/M, and (○) Pt–Fe/M as a function of temperature.

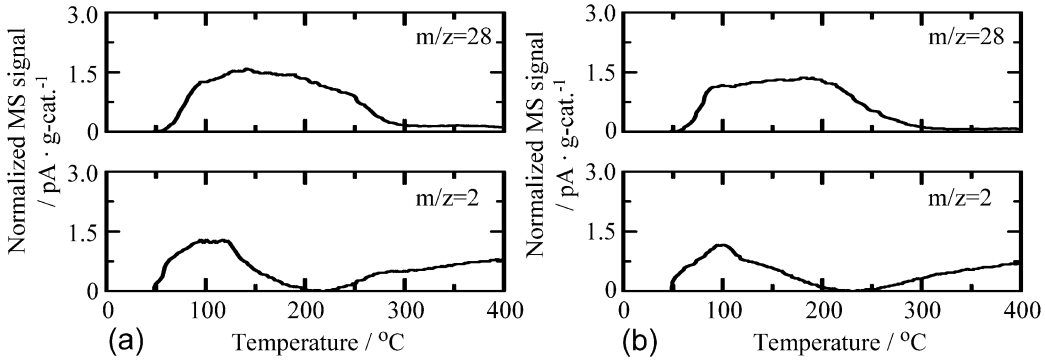

Fig. 5. TPD profiles for CO and H_2 preadsorbed on (a) Pt/M, (b) Pt–Fe/M at 50 °C. Heating rate = 10 °C/min.

3.2.2. *Adsorption property of each metal site at different catalysts*

Fig. 4 shows the adsorption behaviors of Pt/M, Fe/M, and Pt–Fe/M catalysts to pure CO, H_2, and O_2, respectively, as a function of temperature. Fe/M adsorbs neither CO nor H_2 over the whole temperature range examined, but it does adsorb O_2. The amount of adsorbed O_2 increases with increasing temperature. In contrast, Pt/M and Pt–Fe/M catalysts adsorb both CO and H_2 noticeably, in decreasing amounts with increasing temperature. Both catalysts also adsorb O_2 appreciably, in increasing amounts with increasing temperature. The difference in CO and O_2 adsorption between Pt/M and Pt–Fe/M (i.e., Pt–Fe/M adsorbs less CO but more O_2 than Pt/M) should be emphasized. Our previous work on electrocatalysts used in fuel cell anodes demonstrated that Pt–Fe alloy or Pt skin layer of nanothickness formed on Pt–Fe alloy exhibits a low, steady CO coverage (<0.5) in 100-ppm CO/H_2 balance atmosphere even at room temperature, although pure Pt shows the full coverage within a short time. The improved CO tolerance from pure Pt was ascribed to a modification of the electronic structure of Pt sites by the presence of Fe atoms in the vicinity [19,20]. The suppression of CO adsorption seen in Fig. 4a is consistent with that previous observation at electrocatalysis. In contrast, the adsorption of O_2 onto Pt–Fe/M is markedly enhanced by the addition of Fe to Pt/M, as is the preferential O_2 adsorption at Fe/M to Pt/M, as seen in Fig. 4c. This observation also agrees well with our explanation of the enhanced O_2 electroreduction in fuel cell cathodes by alloying Pt with transition d-metals, which can be ascribed to increased O_2 coverage on Pt sites by the increased d-vacancy of the Pt valence band [21]. As Fig. 4b shows, adding Fe to Pt is effective in modifying CO and O_2 adsorption but not H_2 adsorption; that is, the amount of H_2 adsorption on Pt/M and Pt–Fe/M does not differ and is smaller than the amount of CO or O_2 adsorption.

Fig. 5 shows TPD profiles of CO and H_2 preadsorbed on Pt/M (a) and Pt–Fe/M (b) in 0.5% CO, 5% H_2, and He balance at 50 °C, respectively. Desorption of CO ($m/z = 28$) is observed from 50 to 300 °C at Pt/M. Two H_2 desorption peaks ($m/z = 2$) are seen at ca. 100 and over 250 °C. The former was assigned to chemisorbed hydrogen on the metal surface [22]; the latter, to strongly chemisorbed hydrogen [23]. We have not yet qualified the sites for the strongly bonding H_2, but it seems to be not so reactive. Pt–Fe/M shows quite similar TPD profiles to those of Pt/M. The amounts of CO and H_2, as well as their molar ratios, estimated from the desorption peak areas, are not significantly different between Pt/M and Pt–Fe/M (although they are slightly smaller in the latter). Therefore, it is thought that Pt sites in Pt–Fe/M and Pt/M have similar adsorption properties to CO and H_2. In any event, this result indicates that not only CO, but also H_2, can adsorb on the catalyst sites during the practical PROX reaction. Because Fe sites in Fe/M exhibit no affinity to CO and H_2 adsorption, as shown in Figs. 4a and 4b, it is reasonable to consider that CO as well as H_2 adsorb on Pt sites in Pt/M and Pt–Fe/M during the PROX reaction.

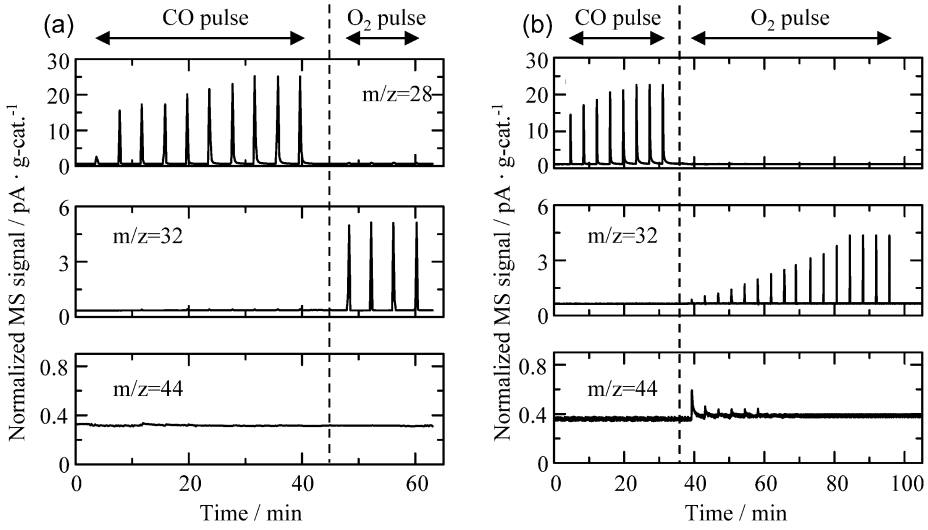

Fig. 6. Reactivity of CO preadsorbed on (a) Pt/M, (b) Pt–Fe/M toward pulse-injected O_2.

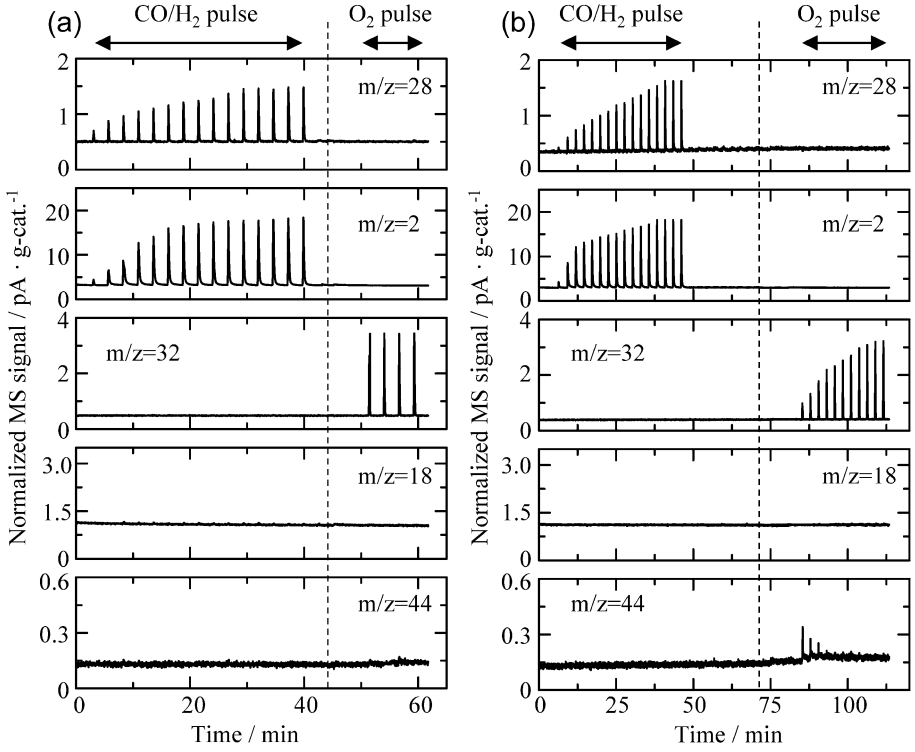

Fig. 7. Reactivity of CO and H_2 competitively preadsorbed on (a) Pt/M, (b) Pt–Fe/M toward pulse-injected O_2.

3.2.3. Reactivity and selectivity of the CO adsorbed on Pt/M and Pt–Fe/M

Fig. 6 shows the results of mass spectrum analyses on the preadsorption of CO and on CO oxidation with pulse-injected O_2 on Pt/M and Pt–Fe/M at 50 °C. In Pt/M (Fig. 6a), the height of the CO peak ($m/z = 28$) increases with increasing pulse time. Finally, its height becomes constant, indicating saturated coverage with CO on Pt sites. After saturation, the catalyst is exposed to O_2 pulses. The height of every detected O_2 peak ($m/z = 32$) is constant, meaning at least that O_2 adsorption does not occur at the Pt sites saturated with CO in Pt/M. Because no CO_2 ($m/z = 44$) formation is observed, no oxidation reaction also occurs. In contrast, at Pt–Fe/M, the initial O_2 pulse height decreases dramatically and forms CO_2 (see Fig. 6b). The pulse height for O_2 increases stepwise and reaches to the full height after 12 pulses and vice versa for CO_2 formation. Thus, it becomes clear that CO molecules adsorbed on Pt sites in Pt–Fe/M are extremely reactive with injected O_2, in contrast to those in Pt/M.

How does the presence of coadsorbed H_2 with CO affect the reactivity and selectivity at the same catalysts? The experimental results are shown in Fig. 7. First, preadsorption of reactant gases on Pt/M and Pt–Fe/M was performed in mixed gas stream (0.5% CO, 5% H_2, and He balance) at 50 °C. Pt/M tends to

achieve the saturated adsorption of CO ($m/z = 28$) and H_2 ($m/z = 2$) more quickly than Pt–Fe/M. After reaching the saturated adsorption, O_2 ($m/z = 32$) pulses are injected in the He carrier stream. Neither CO_2 ($m/z = 44$) nor H_2O ($m/z = 18$) is formed with no consumption of injected O_2 at Pt/M; however, CO_2 is immediately formed at Pt–Fe/M by the oxidation of adsorbed CO with pulse-injected O_2. Nevertheless no H_2O is detected. The results of CO/H_2-TPD in Fig. 5 show the presence of two kinds of H_2. The weakly adsorbed H_2, desorbed completely up to 150 °C, may react with O_2 and formed H_2O. The H_2O is presumably trapped in the mordenite cages and cannot be detected in the present experiment shown in Fig. 7b. We may consider that using strongly adsorbed H_2, starting the desorption at >200 °C, or continuing the desorption at even 400 °C has probably less reactivity to adsorbed O_2 than that of CO, which desorbs completely up to 300 °C. This reasoning can be supported by the result in Figs. 1 and 2 indicating that almost all O_2 was used for the oxidation of CO at 50 °C. The CO adsorbed on Pt sites reacts with O_2 adsorbed on Fe sites, forming CO_2. In the PROX reaction under the steady-state condition, where reactant gases are supplied continuously, such Pt sites as weakly adsorbed H_2 may be occupied with CO preferentially, resulting in the preferential oxidation of CO by the O_2 adsorbed continuously on the neighboring Fe sites. This is the reason why Pt–Fe/M exhibits superior selectivity at such a low operating temperature, despite the presence of a large excess of H_2 compared with CO as well as the added O_2 in reforming gases.

3.2.4. *Mechanisms of the PROX reaction*

Based on the foregoing observations and discussions, we can summarize schematically the adsorption of CO, O_2, and/or H_2 and the reaction processes at the different catalysts, as shown in Fig. 8. As seen in Figs. 6 and 7, no PROX reaction occurs because the reaction sites are fully covered with CO and/or H_2 strongly adsorbed on Pt/M due to blocked access of O_2 to the reaction sites. This strongly indicates that a dissociative adsorption of O_2 and the following surface reaction with preadsorbed CO are essential for the PROX reaction, that is, a Langmuir–Hinshelwood mechanism. The reaction can occur only at Pt/M as the reaction temperature is elevated (>120 °C), maybe because both the CO coverage and the bonding strength are lowered and the resulting CO-free sites are available for the dissociative adsorption of O_2 (see Figs. 1 and 4). But Fe/M has no affinity for CO adsorption, as seen in Fig. 4, presumably because Fe sites are dominantly in FeO phase as indicated by our XANES analysis [18]. As the result, no PROX activity appeared (as seen in Fig. 1), because of the lack of essential requisites for the Langmuir–Hinshelwood mechanism. At Pt–Fe/M, the foregoing results and discussion clearly indicate that Pt sites are available for the adsorption of CO as well as H_2, and that Fe sites act as O_2 adsorption sites. CO adsorbed on a Pt site and O adsorbed on an Fe site react immediately even at 50 °C once both reactants sit on such neighboring sites. This is the mechanism that Watanabe and Motoo proposed as the so-called "bifunctional mechanism" for the electrocatalytic oxidation of "C-containing reactants" on binary alloys such as Pt–Ru [24,25]. A PROX reaction on Au catalysts supported on TiO_2, Al_2O_3, and ZrO_2, an oxidation of CO by H–O–O species, generated via the reaction between dissociatively adsorbed H_2 on the gold particles and O_2 molecule from the gas phase, was suggested [26]. In this mechanism, both CO_2 and H_2 generation must be observed as the result of the reaction between CO and H–O–O species. But when an O_2 pulse was introduced to the Pt–Fe/M catalyst saturated with CO and H_2, CO_2 was formed but H_2 was not detected, as seen Fig. 7b. This experimental result strongly suggests that the PROX reaction on Pt–Fe/M catalyst proceeds not via the pathway proposed for Au-supported catalyst, but via the bifunctional mechanism that we have proposed. Perfect dispersion (or neighborhood) of two types of sites may not be required for the mechanism as long as they are close enough for the surface diffusions of both types to adsorbed reactants. In addition to the components for the bifunctions, the special reaction spaces of zeolite cages are also essential to achieving the desired reactivity and selectivity, as indicated by a performance different than that of the conventional PROX catalysts. A reason why H_2 on Pt sites of Pt/M or Pt–Fe/M is less active than CO at the PROX reaction has not yet been clearly explained, but it does happen and leads to superior selectivity.

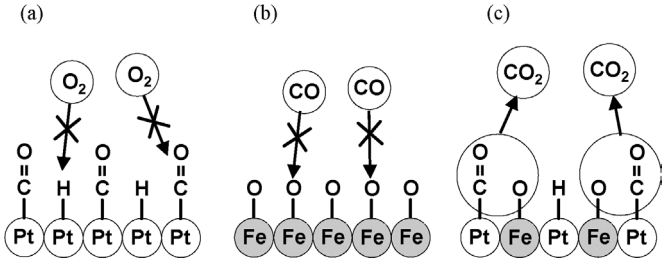

Fig. 8. PROX mechanism, schematically shown, at (a) Pt/M, (b) Fe/M and (c) Pt–Fe/M catalysts.

4. Conclusion

The PROX activity of Pt/M, Fe/M, and Pt–Fe/M was examined. Pt/M and Fe/M did not show any activity at 50 °C. However, Pt–Fe/M showed distinctive PROX reactivity and selectivity at the same temperature—for example, it achieved the ideal performance of 100% at even λ ($2 \times O_2/CO$) = 1.0 and SV = 12,500 h^{-1}, with no noticeable decline in selectivity even at SV = 100,000 h^{-1}. CO, H_2, and O_2 chemisorption measurements demonstrated that Fe/M cannot adsorb CO and H_2, but can absorb O_2, whereas both Pt/M and Pt–Fe/M show a high affinity to both CO and H_2 adsorption. It was also found that adding Fe to Pt/M can preserve O_2 adsorption sites for the PROX reaction even in CO/excess H_2 mixed gas. Regarding the PROX mechanism at low temperatures on Pt/M, Fe/M, and Pt–Fe/M, the poor reactivity of Pt/M and Fe/M can be ascribed to the lack of CO and/or O_2 adsorption as the essential requisite for Langmuir–Hinshelwood mechanism. We proposed the so-called "bifunctional mechanism" for the distinctive performance at Pt–Fe/M, where Pt site acts as CO adsorption site and Fe site acts as an O_2 dissociative-adsorption site and enhances

the surface reaction between the reactants on the neighboring sites.

Acknowledgments

This work was supported by Leading Project of the Administration of Education, Science, Culture and Sports on “Research and Development of Materials for the Next Generation Fuel Cells.”

References

[1] L. Carrette, U. Stimming, Fuel Cells 1 (2001) 5.
[2] R.A. Lemons, J. Power Sources 29 (1990) 251.
[3] B. Hohlein, S.V. Andrian, Th. Grude, R. Menze, J. Power Sources 86 (2000) 243.
[4] M.J. Kahlich, H.A. Gasteiger, R.J. Behm, J. Catal. 171 (1997) 93.
[5] R.M.T. Sanchez, A. Ueda, K. Tanaka, M. Haruta, J. Catal. 168 (1997) 125.
[6] K. Sekizawa, S. Yano, K. Eguchi, H. Arai, Appl. Catal. A 169 (1998) 291.
[7] G.K. Bethke, H.H. Kung, Appl. Catal. A 194/195 (2000) 43.
[8] M. Echigo, T. Tabata, Appl. Catal. A 251 (2003) 157.
[9] H. Tanaka, S. Ito, S. Kameoka, K. Tomishige, K. Kunimori, Catal. Commun. 4 (2003) 1.
[10] M. Echigo, N. Shinke, S. Takami, T. Tabata, J. Power Sources 132 (2004) 29.
[11] P.V. Snytnikov, V.A. Sobyanin, V.D. Belyaev, P.G. Tsyrulnikov, N.B. Shitova, D.A. Shlyapin, Appl. Catal. A 239 (2003) 149.
[12] M. Watanabe, H. Uchida, H. Igarashi, M. Suzuki, Chem. Lett. (1995) 21; JP Patent 07256112;
US Patent 6168772.
[13] H. Igarashi, H. Uchida, M. Watanabe, Chem. Lett. (2000) 1262.
[14] H. Igarashi, H. Uchida, M. Watanabe, Stud. Surf. Catal. 132 (2001) 953.
[15] M. Watanabe, H. Uchida, K. Ohkubo, H. Igarashi, Appl. Catal. B 46 (2003) 595.
[16] M. Kotobuki, A. Watanabe, H. Uchida, H. Yamashita, M. Watanabe, Chem. Lett. (2005) 866.
[17] A. Wootsch, C. Descorme, D. Duprez, J. Catal. 225 (2004) 259.
[18] M. Kotobuki, T. Shido, M. Tada, H. Uchida, H. Yamashita, Y. Iwasawa, M. Watanabe, Catal. Lett. 103 (2005) 263.
[19] M. Watanabe, Y. Zhu, H. Igarashi, H. Uchida, Electrochemistry 68 (2000) 244.
[20] H. Igarashi, T. Fujino, Y. Zhu, H. Uchida, M. Watanabe, Phys. Chem. Chem. Phys. 3 (2001) 306.
[21] T. Toda, H. Igarashi, H. Uchida, M. Watanabe, J. Electrochem. Soc. 146 (1999) 3750.
[22] K. Foger, J.R. Anderson, J. Catal. 54 (1978) 318.
[23] T. Szilagyi, J. Catal. 121 (1990) 223.
[24] M. Watanabe, S. Motoo, J. Electroanal. Chem. 60 (1975) 275.
[25] T. Yajima, H. Uchida, M. Watanabe, J. Phys. Chem. B 108 (2004) 2654.
[26] C. Rossignol, S. Arrii, F. Morfin, L. Piccolo, V. Caps, J. Rousset, J. Catal. 230 (2005) 476.